Quantum dot enabled thermal imaging of optofluidic devices

Lab on a Chip

Cite this: *Lab Chip*, 2012, **12**, 2414–2420

www.rsc.org/loc

PAPER

Quantum dot enabled thermal imaging of optofluidic devices

Debaditya Choudhury,*[a] Daniel Jaque,[b] Airan Rodenas,[a] William T. Ramsay,[a] Lynn Paterson[a] and Ajoy K. Kar[a]

Received 20th February 2012, Accepted 12th March 2012
DOI: 10.1039/c2lc40181a

Quantum dot thermal imaging has been used to analyse the chromatic dependence of laser-induced thermal effects inside optofluidic devices with monolithically integrated near-infrared waveguides. We demonstrate how microchannel optical local heating plays an important role, which cannot be disregarded within the context of on-chip optical cell manipulation. We also report on the thermal imaging of locally illuminated microchannels when filled with nano-heating particles such as carbon nanotubes.

1. Introduction

Temperature is one of the key physical factors governing the fundamental chemical reactions that occur within a live cell. Small changes in temperature can affect intra-cellular dynamics and could also modify the cell's metabolic activity, making it unviable.[1,2] This fact underlies the recent advancements achieved in applying the exceptional optical, thermal and electrical properties of nanoscale materials for therapeutic, imaging and diagnostic biomedical applications.[3,4] Surface functionalized fluorescent semiconductor nanocrystals (Quantum Dots) have far reaching potential as biological probes due to their unprecedented photostability and high sensitivity over long time scales.[4,5] The other rapidly emerging class of biologically significant nanoscale materials are carbon nanotubes (CNT), which absorb energy in the ''tissue-transparent'' near-infrared (NIR) spectrum and are a promising tool for targeted cell hyperthermia.[3] Recent advances in ultrafast laser inscription (ULI) techniques have enabled the creation of optofluidic microenvironments that can be tailored to mimic *in vivo* conditions. A rigorous understanding of the temperature distribution created in microchannels would also enable the evaluation of additional forces that may arise due to the presence of non-negligible thermal gradients such as those leading to photothermal trapping.[6,7] In this paper, we demonstrate the use of these nanomaterials as probes for temperature sensing as well as effectors which act as nano-heaters to understand temperature distribution in microchannels within optofluidic microenvironments. Quantum dots (QD) are used to accurately determine the magnitude, spatial distribution and spectral dependence of laser-induced temperature increments within an optofluidic-integrated chip. This study elucidates how the light-induced thermal loading of microchannels is affected by the presence or absence of absorbing particles (CNT) within the fluid.

The small dimensions of microchannels introduce complications in the accurate determination of their internal temperature. The reduced dimensions of the optically pumped volumes make the use of traditional ''contact'' methods of temperature measurement futile.[8] The requirement of ''remote thermal sensing'' can be realized by recently emerging optical techniques. These are based on the incorporation, within the fluid, of luminescent particles whose luminescence is strongly dependent on temperature in terms of spectral shape, intensity or lifetime.[9,10] Thus, with the help of confocal microscopy, the detailed analysis of the fluid spectral features will provide intra-channel thermal sensing and imaging. The use of fluorescent nanoparticles will also lead to high spatial resolutions significantly improving those achievable by the use of micro-thermocouples. Previous works have reported high-resolution thermal images of fluids using organic compounds such as rhodamine and its derivatives, based on the large temperature-induced variations of their fluorescence intensity and lifetime. The fluorescent compounds were incorporated into the fluid either in the form of a colloidal suspension[11] or by encapsulating within a micro-droplet.[12] These approaches provide 1–2 °C thermal resolution with micron-scale spatial resolution and are capable of thermal imaging in microfluidic environments involving optical traps.[13–15] Despite these excellent results, the use of organic compounds has several drawbacks such as photo-deterioration and low molar absorption coefficient. Both could, in principle, be overcome by the use of CdTe semiconductor quantum dots (CdTe-QDs).[16] Their characteristic fluorescence band that is tunable by QD size,[17] has also very recently been shown to possess an outstanding thermal sensitivity.[18] In particular, for the brightest CdTe-QDs of around 3.8 nm in diameter, the thermal-induced spectral shift is close to 0.35 nm $°C^{-1}$, allowing for temperature resolutions well below 0.5 °C, beating those achieved by other QDs such as CdSe-QDs.[19] In respect to the previously used organic compounds, CdTe-QDs show superior photo-stability, larger molar absorption coefficients,

[a]*SUPA, School of Engineering & Physical Sciences, Heriot-Watt University, Edinburgh, UK. E-mail: A.K.Kar@hw.ac.uk*
[b]*Fluorescence Imaging Group, Departamento de Física de Materiales, Facultad de Ciencias, Universidad Autónoma de Madrid, 28049, Madrid, Spain. E-mail: daniel.jaque@uam.es*

better thermal stability and improved fluorescence quantum yield in the NIR.[16] In addition, CdTe-QDs show a larger two-photon absorption cross-section in such a way that thermal sensing could be achieved under optical excitation within the so-called "biological window" (700 nm–900 nm).[20–24] This, indeed, ensures large penetration depths within the microchannel while minimising the possible presence of auto-fluorescence of the fluid and the thermal loading induced during the thermal imaging procedure. Regardless of these expected benefits, CdTe-QD based fluorescent thermometry has not yet been applied to the study of laser-excited optofluidics.

In this work, we have incorporated CdTe-QDs within an optofluidic device consisting of a microchannel locally illuminated by an adjacent buried waveguide. The laser-induced local heating of the fluid within the microchannel has been determined from the analysis of the spectral position of the CdTe-QDs fluorescence band. To begin with, the validity of CdTe-QDs nano-thermometers was checked by measuring the multi-wavelength laser-induced thermal loading of a water-filled microchannel. Results were compared to those predicted by simple theoretical models for laser-induced heating in optical traps.[25] Subsequently, QD based fluorescence thermometry was applied to determine how laser-induced optofluidic thermal loading is affected by the presence of absorbing particles such as CNTs within the fluid. By analysing the experimental data within the frame of simple theoretical models, we were able to estimate the fraction of the absorption coefficient of CNTs that can be attributed to heat generation. Furthermore, scanning confocal fluorescence imaging was then used to provide the first (to best of our knowledge) two dimensional thermal image of a laser-excited optofluidic device containing absorbing nanoparticles, which are essentially very advanced nano-heaters.

2. Materials and methods

2.1 Optofluidic device

The monolithic device with a microchannel and an optical waveguide was fabricated using the process of ULI followed by selective chemical etching. This technique involves the focusing of femtosecond laser pulses in bulk transparent materials which, depending upon the pulse energy regime, leads to local modification of the material's refractive index as well as enhanced chemical etching selectivity. This allows the simultaneous fabrication of optical waveguides and microchannels with 3D design freedom[26] leading to the fabrication of micro cell-stretchers,[27] sorters[28] and optofluidic sensors.[29] Inscription of the device was performed using 460 fs pulses at 1047 nm from a variable repetition rate, commercial Yb-doped master oscillator power amplifier (IMRA America FCPA μ Jewel), with the repetition rate set at 500 kHz. The pulses were focused using a 0.4 NA (×20) aspheric lens inside a fused silica substrate (Corning 7980, UVFS) that was translated through the laser focus using high precision Aerotech A3200 multi-axis air-bearing stages. As illustrated in Fig. 1a, the device consists of an optical waveguide designed perpendicular to a 5 mm long embedded microchannel with a cross-section of 100 μm × 100 μm that is interfaced with cylindrical inlet and outlet ports, each with an outer diameter of 1 mm. The waveguide was inscribed using the multiscan technique,[30] with each laser scan offset by 0.4 μm,

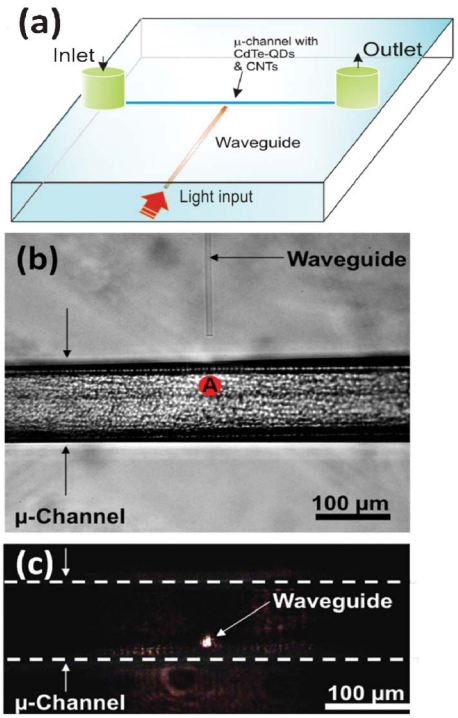

Fig. 1 a) Schematic representation of the thermometry device showing the microchannel and optical waveguide arrangement. b) Top view optical transmission image of the ultrafast laser inscribed device. The 100 μm wide channel as well as the buried waveguide are indicated. Marked point (A) corresponds to the intra-channel location where maximum laser-induced heating was observed and where "single-point" thermal measurements were performed. c) Side view of the ultrafast laser inscribed device when a 633 nm laser was coupled into the buried waveguide. Focal plane was set to be the channel wall nearest to the waveguide.

constructing a geometrical cross-section of 8 μm × 8 μm. The fluidic components were inscribed using 650 nJ linearly polarized pulses and a translation speed of 4 mm s^{-1}, while the waveguide was inscribed using 290 nJ circularly polarized pulses at 2 mm s^{-1}. The inscribed device was subsequently etched for 5 h using hydrofluoric acid at 5% dilution in deionised water. Post etch, the waveguide was polished back to reveal the facet, which was then bonded to a single-channel fibre array (Opteron Co.) using UV curable epoxy (Norland NOA-61) to form a robust, re-usable device. Fig. 1b shows the bright-field optical transmission micrograph of the etched microchannel and optical waveguide that form the device. Fig. 1c shows the side-view of the microchannel with the buried waveguide when light from a 633 nm laser was coupled to it while aligning the fibre-array.

2.2 Confocal fluorescence thermal imaging

For the purpose of thermal imaging and sensing, the optofluidic device was filled with an aqueous solution of CdTe-QDs at a concentration of 0.3% by mass. Once filled, the microchannel was blocked at both ends so there was no flow in the microchannel containing the QD solution. The CdTe-QDs, provided by Plasmachem Inc., were 3.8 nm in diameter and had been surface functionalised using thiocarboxylic acid in such a way that the sulphur binds to Cd in CdTe and –COOH groups are formed surrounding the QDs. As already mentioned,

CdTe-QDs have recently been proposed as very sensitive fluorescent nano-thermometers based on their characteristic temperature-induced spectral shift so that thermal reading is achieved from the accurate determination of the fluorescence peak position.[18] Thermal sensitivity as well as brightness depends on the dot size. The dot size used in this work (3.8 nm) was chosen since it provides a good compromise between these two characteristics.[19,31] For thermal sensing and imaging we used a custom-built confocal fluorescence microscope, which is schematically drawn in Fig. 2a. The optofluidic device was placed on a 10 nm resolution XY motorized stage (PI Hera). A 488 nm beam provided by a CW Argon laser was focused into the microchannel by using a 50× long working distance microscope objective with a numerical aperture of 0.55. The CdTe-QD fluorescence generated from the 488 nm focal point was collected by the same microscope objective and, after passing through appropriate filters and confocal apertures, was analysed spectroscopically by a CCD attached to a high-resolution spectrometer. Integration time for spectrum acquisition was, in all cases, 1 s. The axial and lateral resolutions of our confocal fluorescence system have been estimated to be 3.6 μm and 0.6 μm, respectively. Fig. 2b shows a typical CdTe-QD emission spectrum obtained in our confocal microscope when the 488 nm beam was focused inside the microchannel. In this figure, we indicate the location of the emission peak as well as the relation between its spectral position and the QD temperature increment with respect to room temperature (25 °C).[18] Finally, the local heating produced by the presence of absorbing nano-centres in the solution has been evaluated by incorporating, into the aqueous solution of CdTe-QDs, single-wall carbon nanotubes provided by Sigma Aldrich Ltd. with a concentration of 0.1% by mass.

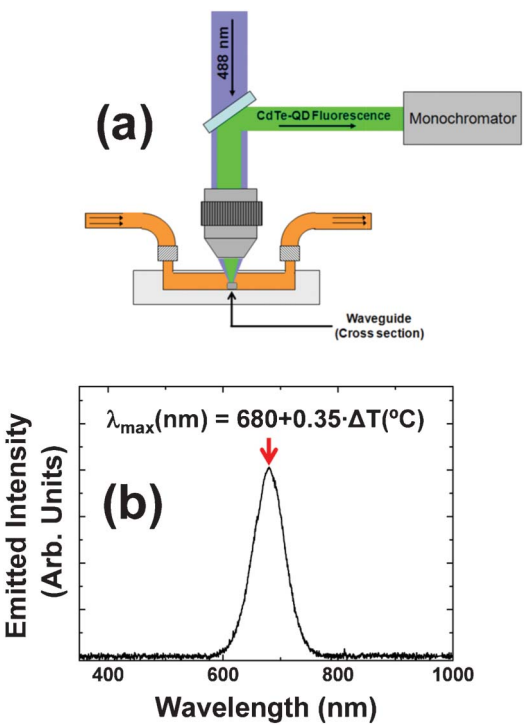

Fig. 2 a) Schematic diagram of the confocal microscope used for fluorescence thermal sensing and imaging in the optofluidic device. b) Typical intra-channel CdTe-QD emission spectrum obtained in our experimental set-up. The location of the peak wavelength and its relation with temperature change (with respect to 25 °C) is indicated.

During thermal imaging, laser-induced thermal gradients were generated by coupling into the buried waveguide either a 980 nm or 1090 nm laser radiation provided by a diode laser or a Yb-doped glass fibre laser, respectively. In both cases, the maximum power launched into the optofluidic device was close to 600 mW. Pump power was, in both cases, controlled through the laser drive current.

3. Results and discussion

3.1 Influence of pump wavelength on the optofluidic thermal loading

One of the most promising applications of optofluidic devices is the achievement of intra-channel optical trapping. Due to the non-vanishing absorption coefficients of water in the NIR, optical trapping in an aqueous environment is accompanied by laser-induced local heating.[32,33] A theoretical prediction, assuming a cylindrical geometry for heat generation and dissipation, predicts that the laser-induced temperature increment at focus, ΔT, in a liquid can be written as:[25]

$$\Delta T = (P_{in}\cdot\alpha_{abs}/2\pi K)\cdot\ln\,(D/w) \quad (1)$$

where P_{in} is the laser power reaching the liquid, α_{abs} is the absorption coefficient of the liquid at the laser wavelength, K is the thermal conductivity of the liquid, D is the shortest dimension of the micro-chamber containing the liquid along the light path, and w is the laser beam waist. The absorption coefficient (α_{ext}) is given by $\alpha_{ext} = \alpha_{sct} + \alpha_{abs}$, where α_{sct} is the scattering coefficient. For the case of distilled water, where light scattering can be neglected, we can assume $\alpha_{ext} = \alpha_{sct} + \alpha_{abs} \approx \alpha_{abs}$. The absorption coefficient of distilled water is shown in Fig. 3 (a). It is evident that the use of trapping wavelengths above 800 nm will be accompanied by some local heating and this has been widely reported in the literature.[11,32–35] In this section, we will take advantage of this effect to explore the ability of QD based thermometry for the determination of laser-induced local heating effects in optofluidics.

The launched laser light travels through a length of optical fibre, the single-channel fibre array and finally the buried ULI waveguide before reaching the microchannel. Due to coupling mismatch between the single-channel fibre array and the waveguide, the net laser power reaching the microchannel (P_{in}) could differ by a large extent from the initial laser power launched into the system (P_{laser}). In order to determine the actual ratio between P_{in} and P_{laser} we first measured the 1090 nm laser-induced heating rate with respect to P_{laser}. We obtained a heating rate of $\Delta T/\Delta P_{laser}$ (1090 nm) = 3.1 °C W^{-1}. This value can be compared to the 1090 nm laser-induced heating rate (with respect to P_{in}) predicted by eqn (1) and experimentally corroborated by Ebert *et al.*:[11] $\Delta T/\Delta P_{in}$ (1090 nm) ≈ 12 °C W^{-1}. Comparing both magnitudes, we can extract the ratio $P_{in}/P_{laser} \approx 0.25$. Once this ratio is known

it is possible to analyse heating rates with respect to the laser power reaching the microchannel.

In order to check the efficacy of the QD based thermometry as well as the validity of the laser power calibration procedure, we have investigated the laser-induced local heating produced when the microchannel is optically excited at 980 mm. At this wavelength, as can be observed in Fig. 3 (a), the water absorption coefficient peak reaches 0.5 cm^{-1}, more than twice the absorption coefficient at 1090 nm. Therefore, a larger local heating is expected under 980 nm excitation. Fig. 3(b) shows the microchannel temperature measured at the closest point to the waveguide indicated by point A in Fig. 1b. It is evident that the microchannel temperature increases linearly with the laser power, in agreement with eqn (1).[25] From the data included in Fig. 3(b) we have estimated a heating rate of $\Delta T/\Delta P_{in}$ at 980 nm $\approx$ 55 °C W^{-1}. This value can be compared to the one theoretically calculated by using eqn (1) that yields $\Delta T/\Delta P_{in}$ (980 nm) = 45 °C W^{-1},[25] therefore there is a reasonable agreement between experimental data and theoretical predictions. The laser-induced heating rate at 980 nm obtained here can also be compared, within a first order approximation, to that previously reported by Mao *et al.* in an optical tweezers system.[25] They found a 980 nm laser-induced heating rate of 56 °C W^{-1} that is, indeed, in excellent agreement with our experimental results.

The results described in this section clearly confirm CdTe-QD thermometry as a valid approach for fluorescence thermal imaging of optofluidic devices. This fact suggests its use for thermal imaging of laser-excited optofluidics containing absorbing centres, as demonstrated in Section 3.2.

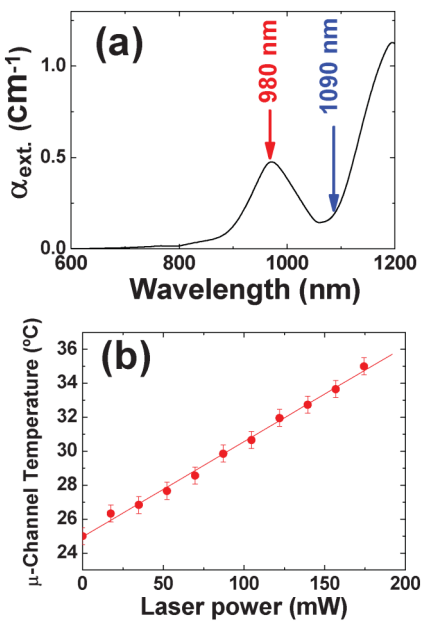

Fig. 3 a) Room temperature absorption spectrum of distilled water in the 800–1200 nm range. Arrows indicate the absorption coefficients for the two laser wavelengths used in this work (980 and 1090 nm). b) Local temperature as measured at point A within the microchannel (see Fig. 1 (b)) as a function of 980 nm laser power reaching the microchannel.

3.2 Thermal loading of an optofluidic device containing absorbing nanoparticles

Although laser-induced heating is usually regarded as an undesirable effect, in many applications laser-induced heating is a desirable effect that should be maximised. This is the case, as indicated earlier, of light-induced cell hyperthermia. In this case, controlled heating of a trapped cell is required for targeted cell death or for the study of the thermal dependence of cell properties such as elasticity, growth and division rates and membrane stability.

One approach to achieve this controlled cellular hyperthermia consists of the inclusion of heat-absorbing nanoparticles in the fluid containing the cells. CNTs are known to induce relevant heating when optically illuminated in the infrared, therefore acting as nano-heaters.[35–38] Nevertheless, to the best of our knowledge, the magnitude and spatial distribution of the laser-induced temperature variations induced by CNTs in an optofluidic device is still unknown. For that purpose, an aqueous solution of both CdTe-QDs and CNTs (0.3 and 0.1% by mass, respectively) was injected into our optofluidic device. The absorption spectrum of the CdTe-QDs and CNT solution is shown in Fig. 4a. The absorption spectrum of an aqueous solution of CdTe-QDs (0.3% by mass) is also included for the sake of comparison. As can be observed, the presence of CNTs increases the optical absorption of the solution, in agreement with previous works on CNTs, reporting a broad absorption band extending from the visible to the infrared.[36–38] In particular, the presence of CNTs increases the absorption coefficient at 1090 nm from 0.21 up to 5.3 cm^{-1} *i.e.* almost by

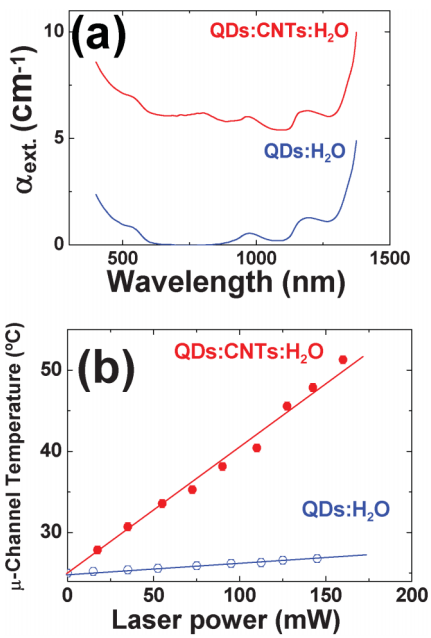

Fig. 4 a) Room temperature absorption spectrum of an aqueous solution containing CdTe-QDs in the presence and absence of CNTs in distilled water. b) Local temperature at point A (see Fig. 1(b)) as a function of 1090 nm laser delivered power when the microchannel was filled with a solution containing CNTs. Data obtained for the same solution in the absence of CNTs is also included for the sake of comparison.

a factor of 20. This increment is attributed to the non-vanishing absorption of CNTs in this spectral range as well as to the light scattering induced by CNTs. Thus, the 1090 nm laser-induced thermal loading of the optofluidic device is expected to be significantly enhanced due to the presence of CNTs. This is, indeed, what we have observed. Fig. 4b shows the microchannel temperature measured at the closest point to the waveguide indicated by point A in Fig. 1b, in the presence and absence of CNTs. In both cases a linear relation has been obtained, as predicted by eqn (1). In the presence of CNTs the heating rate has been found to be as large as $\Delta T/\Delta P_{laser}$ (1090 nm, CNT) = 160 °C W^{-1}, *i.e.* more than 10 times the heating rate found in pure water (without CNTs). From the experimentally determined heating rate and taking advantage of eqn (1) it is possible to estimate the absorption coefficient of CNTs at 1090 nm. We have obtained α_{abs} (1090 nm, CNT) ≈ 2.4 cm^{-1}. When compared to the absorption coefficient at this wavelength (α_{ext}.(1090 nm, CNT) ≈ 5.8 cm^{-1}) this reveals a noticeable scattering contribution to the absorption coefficient of CNT at this wavelength. Indeed, scattering accounts for more than 50% of the optical absorption of CNTs at 1090 nm. Appreciable relative scattering contributions to the absorption coefficient have been also observed for other heating nanoparticles such as gold nano-rods of large aspect ratios.[39] Thus, from data included in Fig. 4b it is evident that CNTs could induce intra-channel temperatures well in excess of those required for targeted cell hyperthermia (above 45 °C), even by using moderate 1090 nm laser powers of 150 mW.

As mentioned before, for practical applications it is vital to know the maximum induced thermal heating of the optofluidic device as well as its spatial distribution. This requires the acquisition of thermal images of the microchannel in the presence of the laser radiation. Such thermal imaging is also possible with the aforementioned QD based thermometry. For that purpose we scanned the optofluidic device by varying the 488 nm focus spot within the microchannel. For each point, the spectral position of CdTe-QDs emission peak was determined so that a fluorescence image of the microchannel was obtained in terms of emission shift. The fluorescence image was then translated into temperature units by taking into account the temperature coefficient of the CdTe-QDs fluorescence band (0.35 nm $°C^{-1}$, in our case). This enabled us to obtain thermal images as shown in Fig. 5a, showing the spatial temperature variation induced in the microchannel filled with the CdTe-QD and CNT solution, when 38 mW of 1090 nm radiation was launched into the microchannel. Fig. 5a reveals how the temperature reaches a maximum where the intra-channel photon density peaks along the propagation path of the laser radiation delivered by the waveguide. From this thermal image it is possible to estimate the heat-affected zone. Fig. 5b shows the microchannel temperature profile obtained along the dashed line indicated in the thermal image of Fig. 5a. This profile shows that although the 1090 nm laser beam is expected to be well localized within the microchannel, the temperature variation extends over tens of microns, due to the presence of heat diffusion processes. In addition to the determination of the heat-affected zone, the temperature profile included in Fig. 5 also reflects the thermal and spatial resolution achieved using this on-chip thermometry method. It is important to note that temperature oscillations

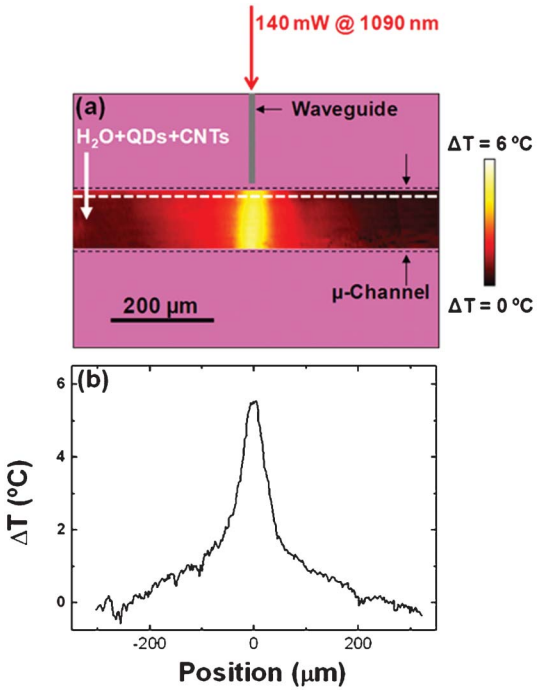

Fig. 5 a) Thermal image of a microchannel filled with an aqueous solution of CdTe-QDs and CNTs when optically excited at 1090 nm. The laser power reaching the microchannel was 38 mW. b) Thermal profile obtained along the horizontal scan-path indicated by the dashed line in part a.

attributed to noise *i.e.* thermal uncertainty is well below 0.2 °C, constituting an outstanding thermal sensitivity.

The outstanding sensitivity of CdTe-QDs can be used to monitor weak variations of temperature along the microchannel, such as those produced along the beam propagation path. The absorption coefficient of the CNT solution at 1090 nm is 5.8 cm^{-1} (see Fig. 4a). In accordance with the Beer–Lambert law, this should result in the reduction of about 5% in the beam intensity along its path across the 100 μm wide microchannel. This in turn, would lead to a small (≈ 5%) reduction in the on-axis temperature. Fig. 6 shows the variation of temperature

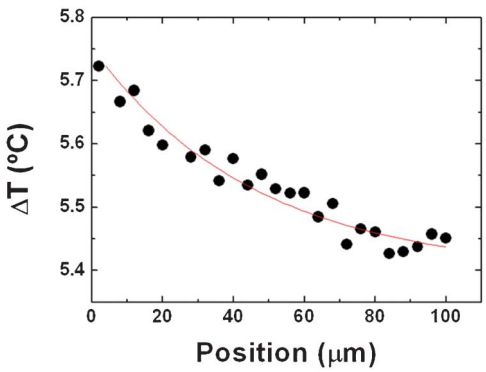

Fig. 6 Temperature variation along the 1090 nm laser beam path as obtained from Fig. 5a. Dots are experimental data and the solid line is a guide for the eyes. Positions x = 0 and 100 μm correspond to the input and output faces of the microchannel along the beam path, respectively for a 1090 nm laser power of 38 mW.

along the laser beam path within the microchannel obtained from the thermal image of Fig. 5a. The position $x = 0$ refers to the input face of the microchannel whereas the position $x =$ 100 μm corresponds to the output face. As expected, the temperature decreases monotonously along the beam path. The total temperature reduction across the microchannel is close to 4%, in good agreement with the estimation made on the basis of the Beer–Lambert law.

4. Conclusion

QD thermometry has been applied to obtain high-resolution spatio-thermal images of the phenomenon of increased thermal loading within an optofluidic device due to the presence of absorbing nanoparticles such as carbon nanotubes. This work incorporates the powerful techniques of ultrafast laser inscription and semiconductor quantum dot thermometry allowing the creation of a non-intrusive temperature sensor platform for laser-excited, optofluidic microenvironments.

Acknowledgements

Debaditya Choudhury is funded by a Heriot-Watt University Life Science Interface Theme Scholarship. William T. Ramsay acknowledges funding from the UK Engineering and Physical Sciences Research Council (EPSRC). Airan Rodenas acknowledges financial support from the Spanish Ministerio de Educación under the Programa de Movilidad de Recursos Humanos del Plan Nacional de I+D+I 2008/2011 for abroad postdoctoral researchers. The authors wish to acknowledge EPSRC (grant number EP/G030227/1) for the IMRA FCPA μJewel femtosecond laser MOPA system. The authors also wish to acknowledge Kevin Prior for facilitating the HF etching capabilities of the group and Peter Heron for prompt technical support. Daniel Jaque thanks Caja Madrid Foundation for the Exchange Scholarship and MICIIN for financial support through project 2010-16161.

References

1 R. I. Morimoto, Cells in stress: transcriptional activation of heat shock genes, *Science*, 1993, **259**, 1409–1410.
2 F. Wetzel, S. Ronicke, K. Muller and M. Gyger, Single cell viability and impact of heating by laser absorption, *Eur. Biophys. J.*, 2011, **40**, 1109–1114.
3 K. Kostarelos, A. Bianco and M. Prato, Promises, facts and challenges for carbon nanotubes in imaging and therapeutics, *Nat. Nanotechnol.*, 2009, **4**, 627–633.
4 I. L. Medintz, H. T. Uyeda, E. R. Goldman and H. Mattoussi, Quantum dot bioconjugates for imaging, labelling and sensing, *Nat. Mater.*, 2005, **4**, 435–446.
5 R. Hardman, A Toxicologic Review of Quantum Dots: Toxicity Depends on Physicochemical and Environmental Factors., *Environ. Health Perspect.*, 2006, **114**, 165–172.
6 H. R. Jiang, H. Wada, N. Yoshinaga and M. Sano, Manipulation of Colloids by a Nonequilibrium Depletion Force in a Temperature Gradient, *Phys. Rev. Lett.*, 2009, **102**, 208301–208305.
7 H. Xin, X. Li and B. Li, Massive photothermal trapping and migration of particles by a tapered optical fiber, *Opt. Express*, 2011, **19**, 17065–17074.
8 J. Lee and N. A. Kotov, Thermometer design at the nanoscale, *Nano Today*, 2007, **2**, 48–51.
9 C. D. S. Brites, P. P. Lima, N. J. O. Silva, A. Millan, V. S. Amaral, F. Palacio and L. D. Carlos, Lanthanide-based luminescent molecular thermometers, *New J. Chem.*, 2011, **35**, 1177–1183.
10 C. D. S. Brites, P. P. Lima, N. J. O. Silva, A. Millan, V. S. Amaral, F. Palacio and L. D. Carlos, A Luminescent Molecular Thermometer for Long-Term Absolute Temperature Measurements at the Nanoscale, *Adv. Mater.*, 2010, **22**, 4499–4504.
11 S. Ebert, K. Travis, B. Lincoln and J. Guck, Fluorescence ratio thermometry in a microfluidic dual-beam laser trap., *Opt. Express*, 2007, **15**, 15493–15499.
12 M. A. Bennet, P. R. Richardson, J. Arlt, A. McCarthy, G. S. Buller and A. C. Jones, Optically trapped microsensors for microfluidic temperature measurement by fluorescence lifetime imaging microscopy, *Lab Chip*, 2011, **11**, 3821–3828.
13 E. M. Graham, K. Iwai, S. Uchiyama, A. Prasanna de Silva, S. W. Magennis and A. C. Jones, Quantitative mapping of aqueous microfluidic temperature with sub-degree resolution using fluorescence lifetime imaging microscopy, *Lab Chip*, 2010, **10**, 1267–1273.
14 S. W. Magennis, E. M. Graham and A. C. Jones, Quantitative Spatial Mapping of Mixing in Microfluidic Systems, *Angew. Chem., Int. Ed.*, 2005, **44**, 6512–6516.
15 R. K. P. Benninger, Y. Koc, O. Hofmann, J. Requejo-Isidro, M. A. A. Neil, P. M. W. French and A. J. deMello, Quantitative 3D Mapping of Fluidic Temperatures within Microchannel Networks Using Fluorescence Lifetime Imaging, *Anal. Chem.*, 2006, **78**, 2272–2278.
16 U. Resch-Genger, M. Grabolle, S. Cavaliere-Jaricot, R. Nitschke and T. Nann, Quantum dots versus organic dyes as fluorescent labels, *Nat. Methods*, 2008, **5**, 763–775.
17 Y. Masumoto and K. Sonobe, Size-dependent energy levels of CdTe quantum dots, *Phys. Rev. B: Condens. Matter*, 1997, **56**, 9734–9737.
18 L. M. Maestro, C. Jacinto, U. R. Silva, F. Vetrone, J. A. Capobianco, D. Jaque and J. Garcia Sole, CdTe Quantum Dots as Nanothermometers: Towards Highly Sensitive Thermal Imaging, *Small*, 2011, **7**, 1774–1778.
19 L. M. Maestro, E. M. Rodriguez, F. Sanz-Rodriguez, M. C. Iglesias-de la Cruz, A. Juarranz, R. Naccache, F. Vetrone, D. Jaque, J. A. Capobianco and J. Garcia Sole, CdSe Quantum Dots for Two-Photon Fluorescence Thermal Imaging, *Nano Lett.*, 2010, **10**, 5109–5115.
20 D. R. Larson, W. R. Zipfel, R. M. Williams, S. W. Clark, M. P. Bruchez, F. W. Wise and W. W. Webb, Water-Soluble Quantum Dots for Multiphoton Fluorescence Imaging *in Vivo*, *Science*, 2003, **300**, 1434–1436.
21 K. Konig, Multiphoton microscopy in life sciences., *J. Microsc.*, 2000, **200**, 83–104.
22 V. Venugopalan, N. S. Nishioka and B. B. Mikic, Thermodynamic response of soft biological tissues to pulsed infrared-laser irradiation, *Biophys. J.*, 1996, **70**, 2981–2993.
23 M. K. So, C. Xu, A. M. Loening, S. S. Gambhir and J. Rao, Self-illuminating quantum dot conjugates for in vivo imaging, *Nat. Biotechnol.*, 2006, **24**, 339–343.
24 L. M. Maestro, J. E. Ramirez-Hernandez, N. Bogdan, J. A. Capobianco, F. Vetrone, J. Garcia Sole and D. Jaque, Deep tissue bio-imaging using two-photon excited CdTe fluorescent quantum dots working within the biological window, *Nanoscale*, 2012, **4**, 298–302.
25 H. Mao, J. R. Arias-Gonzalez, S. B. Smith Jr., I. Tinoco and C. Bustamante, Temperature Control Methods in a Laser Tweezers System, *Biophys. J.*, 2005, **89**, 1308–1316.
26 M. Kim, D. J. Hwang, H. Jeon, K. Hiromatsu and C. P. Grigoropoulos, Single cell detection using a glass-based optofluidic device fabricated by femtosecond laser pulses, *Lab Chip*, 2009, **9**, 311–318.
27 N. Bellini, K. C. Vishnubhatla, F. Bragheri, L. Ferrara, P. Minzioni, R. Ramponi, I. Christiani and R. Osellame, Femtosecond laser fabricated monolithic chip for optical trapping and stretching of single cells, *Opt. Express*, 2010, **18**, 4679–4688.
28 D. Choudhury, W. T. Ramsay, R. Kiss, N. A. Willoughby, L. Paterson and A. K. Kar, A 3D mammalian cell separator biochip, *Lab Chip*, 2012, **12**, 948–953.
29 V. Maselli, J. R. Grenier, S. Ho and P. R. Herman, Femtosecond laser written optofluidic sensor: Bragg grating waveguide evanescent probing of microfluidic channel, *Opt. Express*, 2009, **17**, 11719–11729.
30 N. D. Psaila, R. R. Thomson, H. T. Bookey, N. Chiodo, S. Shen and R. Osellame, Er:Yb-Doped Oxyfluoride Silicate Glass Waveguide Laser Fabricated Using Ultrafast Laser Inscription, *IEEE Photonics Technol. Lett.*, 2008, **20**, 126–128.

31 L. M. Maestro, C. Jacinto, U. Rocha, M. C. Iglesias-de la Cruz, F. Sans-Rodriguez, A. Juarranz, J. Garcia Sole and D. Jaque, Optimum quantum dot size for highly efficient fluorescence bioimaging, *J. Appl. Phys.*, 2012, **111**, 023513.
32 E. J. G. Peterman, F. Gittes and C. F. Schmidt, Laser-Induced Heating in Optical Traps., *Biophys. J.*, 2003, **84**, 1308–1316.
33 Y. Liu, D. K. Cheng, G. J. Sonek, M. W. Berns, C. F. Chapman and B. J. Tromberg, Evidence for localized cell heating induced by infrared optical tweezers, *Biophys. J.*, 1995, **68**, 2137–2144.
34 P. M. Celliers and J. Conia, Measurement of Localized Heating in the Focus of an Optical Trap, *Appl. Opt.*, 2000, **39**, 3396–3407.
35 C. Iancu and L. Mocan, Advances in cancer therapy through the use of carbon nanotube-mediated hyperthermia, *Int. J. Nanomed.*, 2011, **6**, 1675–1684.
36 J. R. Whitney, S. Sarkar, J. Zhang, T. Do, T. Young, M. K. Manson, T. A. Campbell, A. A. Puretzky, C. M. Rouleau, K. L. More, D. B. Geohegan, C. G. Rylander, H. C. Dorn and M. N. Rylander, Single walled carbon nanohorns as photothermal cancer agents, *Lasers Surg. Med.*, 2011, **43**, 43–51.
37 F. Zhou, D. Xing, Z. Ou, B. Wu, D. E. Resasco and W. R. Chen, Cancer photothermal therapy in the near-infrared region by using single-walled carbon nanotubes, *J. Biomed. Opt.*, 2009, **14**, 021009.
38 Z. M. Markovic, L. M. Harhaji-Trajkovic, B. M. Todorovic-Markovic, D. P. Kepic, K. M. Arsikin, S. P. Jovanovic, A. C. Pantovic, M. D. Dramicanin and V. S. Trajkovic, In vitro comparison of the photothermal anticancer activity of graphene nanoparticles and carbon nanotubes, *Biomaterials*, 2011, **32**, 1121–1129.
39 P. K. Jain, K. S. Lee, I. H. El-Sayed and M. A. El-Sayed, Calculated Absorption and Scattering Properties of Gold Nanoparticles of Different Size, Shape, and Composition: Applications in Biological Imaging and Biomedicine, *J. Phys. Chem. B*, 2006, **110**, 7238–7248.